Journal of Alloys and Compounds 522 (2012) 123–129

Contents lists available at SciVerse ScienceDirect

Journal of Alloys and Compounds

journal homepage: www.elsevier.com/locate/jallcom

Enhancement of localization phenomena driven by covalency in the $SrBiMn_{1.75}Ti_{0.25}O_6$ manganite

E. Asensio de Lucas[a], I. Álvarez-Serrano[a], G.J. Cuello[b], M. García-Hernández[c], M.L. López[a,*], C. Pico[a], M.L. Veiga[a]

[a] Depto. Química Inorgánica I, Facultad Ciencias Químicas, Universidad Complutense de Madrid, E-28040 Madrid, Spain
[b] Institut Laue-Langevin, 6 rue Jules Horowitz, F-38042 Grenoble , France
[c] Instituto de Ciencia de Materiales de Madrid, CSIC, E-28049 Cantoblanco, Madrid, Spain

ARTICLE INFO

Article history:
Received 26 September 2011
Accepted 20 January 2012
Available online 1 February 2012

Keywords:
Manganites
Bismuth
Charge ordering
Orbital ordering
Neutron diffraction

ABSTRACT

Manganites are materials that show remarkable phenomena related to charge orbital ordering (CO/OO) and it is extremely important to understand the fundamental nature of this behaviour. This paper reports on the structural, electronic and magnetic behaviour of the new $SrBiMn_{1.75}Ti_{0.25}O_6$ manganite and the dependence of these properties with temperature. A detailed structural analysis has been carried out by electron, X-ray, neutron diffraction between 4 and 700 K. The electron diffraction patterns obtained at room temperature (RT) evidence that the average structure ($a \sim b \sim \sqrt{2}a_p$ and $c \sim 2a_p$) presents a modulation that doubles the *a* and *c* lattice parameters. A very high charge ordering (CO) transition temperature of 510 K, similar to that found for the non-doped material, $SrBiMn_2O_6$, is observed. Above this temperature the symmetry changes from orthorhombic to tetragonal. The conductivity and susceptibility data show a strong interdependence with the structural transition. The activation energy decreases from 0.24 eV to 0.12 eV below and above 510 K, respectively. On the other hand, the high value of the magnetic moment ($\mu_{eff} = 9.34\ \mu_B$), observed between 300 and 500 K, is interpreted in terms of the existence of Mn_4 magnetic clusters. Finally, extra maxima appearing in neutron diffraction patterns at lower temperatures are interpreted considering the stabilization of AFM interactions, consistent with an A-type magnetic ordering. The results are discussed in the framework of charge ordering/orbital ordering and cluster models.

1. Introduction

The mixed valent manganites are a subject of intense applied and basic research due to their spin-dependent properties [1]. Moreover, in these mixed oxides the electronic-type transitions related to charge localization, orbital ordering (OO) assisted by the Jahn-Teller (J-T) effect, and charge ordering (CO) are being currently investigated [1–8].

The CO was first established in the $La_{1-x}Ca_xMnO_3$ series [9,10] with $x \sim 0.5$ as an 1:1 ordering of Mn^{3+} and Mn^{4+} species. In general, this CO is associated with OO due to the cooperative J-T distortion that comes from Mn^{3+} cations. Therefore, the transport properties are often interpreted as the combined influence of CO and OO. These effects have been more recently discussed in different $R_{1-x}A_xMnO_3$ manganites (*R* = rare earth [11–16] or Bi [17–22] and *A* = Ca, Sr). In $Ln_{1-x}Ca_xMnO_3$ (*Ln* = lanthanoid element) oxides, that exhibit an orthorhombic *Pbnm* structure (with the cell parameters close to $\sqrt{2}a_p \times \sqrt{2}a_p \times 2a_p$) at room temperature (RT), the CO state is characterized by a doubling of the *a* parameter and appears at low temperature. In the $Ln_{1-x}Sr_xMnO_3$ manganites, the size of the *Ln* cations plays a drastic role on the RT structures [2,3], involving different types of cell distortions (*Pnma*, *Imma* or *I2/a*, *I4/mcm* or $R\bar{3}c$) as the Ln^{3+} mean ionic radius increases. Moreover, at low temperature, complex structural and magnetic coupled transitions have been evidenced from electron and neutron diffraction data [5–8,12,13,23]. Other previous studies reported on the bismuth-based manganites show that in the $Bi_{1-x}A_xMnO_3$ oxides, in which *A* = Ca and Sr, charge ordering is stabilized up to much higher temperatures [24,25]. Besides, in the $Ln_{½}A_{½}MnO_3$ series the evolution of T_{CO} [26,27] seems to be related to the average tilting of the octahedra and therefore with the <Mn—O—Mn> mean angle. However, in the Sr and Bi-containing systems the highly polarisable $6s^2$ lone pair of Bi^{3+} seems to play an active role in the high T_{CO}, as observed for $Bi_{1-x}Sr_xMnO_3$ family [19]. In fact, this stereochemically active $6s^2$ lone pair combined with the possible magnetic interactions provided by the 3d paramagnetic cations, have renewed attention in these systems, due to the great interest in multiferroic materials and potential applications as solid oxide fuel cells (SOFCs) materials [28].

* Corresponding author. Tel.: +34 1 394 4349; fax: +34 1 394 4352.
E-mail address: marisal@quim.ucm.es (M.L. López).

0925-8388/$ – see front matter © 2012 Elsevier B.V. All rights reserved.
doi:10.1016/j.jallcom.2012.01.124

In contrast to the above $R_{1-x}A_xMnO_3$ (R = rare earth or Bi, and A = Ca, Sr) phases, the manganites in which the Mn is substituted by other transition metal have been scarcely studied. For instance, when nickel is introduced at the perovskite B sites in the $Bi_{0.5}Ca_{0.5}MnO_3$ compound an almost linear decrease of T_{CO} as a function of doping level is observed [29]. Similar results were obtained when doping is made with chromium instead of nickel [30]. For the $Bi_{0.5}Ca_{0.5}Mn_{0.9}Ni_{0.1}O_3$ phase it was concluded that the CO state became suppressed and the Curie constants suggested the existence of Mn_xNi_y magnetic clusters around Ni^{2+}. These facts are interpreted as a competition between ferromagnetic and antiferromagnetic inter-cluster interactions giving rise to a glassy magnetic behaviour [29].

With the aim of exploring the unknown $SrBiMn_{1.75}Ti_{0.25}O_6$ phase we report here an investigation of the temperature-dependent electronic and magnetic behaviour of this phase. Based on electron, X-ray and neutron diffraction measurements between 4 and 700 K, our data confirm that the CO transition temperature found for the non doped material, i.e. $SrBiMn_2O_6$, remains very high in despite of the introduction of Ti cations at the B sites. The results are discussed in the framework of CO/OO and cluster models.

2. Experimental

Polycrystalline powders of the $SrBiMn_{1.75}Ti_{0.25}O_6$ perovskite were prepared by the "liquid-mix" method using stoichiometric amounts of $Sr(NO_3)_2$, $Bi_5O(OH)_9(NO_3)_4$, $TiC_{10}H_{14}O_5$ (Merck chemicals) and $Mn(C_2H_3O_2)_3{\cdot}2H_2O$ (Aldrich chemicals). These reactants were dissolved in a 20% (v/v) HNO_3 solution and after citric acid (a concentration up to 1 M) and ethyleneglycol (5%, v/v) were added. The resulting solution was heated at 523 K until a brown gel was obtained. Then several thermal treatments at 573, 673 and 773 K were applied in order to decompose the organic residues. Finally, the samples were heated in accumulative treatments until a temperature of 1173 K for 12 h, with intermediate grindings. The product was a black powder, later identified as a pure phase. Typical grain sizes ranging between 200 and 800 nm were observed in scanning microscopy images.

X-ray powder diffraction patterns were obtained at selected temperatures, from room temperature to 700 K, with a Siemens D-5000 diffractometer using Cu(Kα) radiation with λ = 1.5418 Å. Neutron diffraction patterns (NDP) were recorded at 4, 150, 300 and 700 K in the high resolution D2B diffractometer at ILL (Grenoble, France). A wavelength of 1.594 Å was selected from a germanium monochromator. The counting time was 4 h using about 4 g of sample contained in vanadium and silica cans (for low and high temperature experiments, respectively). The collected data were analyzed by the Rietveld [31] profile method using the Fullprof program [32].

High resolution transmission electron microscopy (HRTEM) and electron diffraction (ED) were performed using a PHILIPS CM300FEG super-twin. Samples were prepared by crushing the powders under *n*-butanol and dispersing them over copper grids covered with a holey carbon film. Semiquantitative chemical analyses were made from energy dispersive X-ray spectroscopy (EDS).

The d.c. magnetization data were measured with a SQUID (Quantum Design, MPMS-XL model), in the temperature range 4.2–700 K, in an applied field of 500 Oe. Isothermal magnetization measurements have been made up to 6 T at 5 K.

The d.c. conductivity results were obtained on pressed pellets using a four-probe apparatus according to the Van der Pauw method, in the temperature range 108–762 K. Colloidal platinum paint was used to make the contacts.

3. Results and discussion

3.1. Electron diffraction analysis

The composition of the title compound was checked by EDS analysis averaging over a large number of crystallites. These analyses confirmed the expected cationic stoichiometry. Electron diffraction (ED) patterns, on numerous crystallites, clearly showed that the sample was monophasic and the reflections could be indexed by considering an orthorhombic distorted perovskite subcell with $a \sim b \sim \sqrt{2}a_p$ and $c \sim 2a_p$ (where a_p is the cell parameter of the ideal simple cubic perovskite). ED patterns along some zone axes are given in Fig. 1.

The obtained reflections conditions are consistent with an *I*-type cell since in the viewing direction, no *hkl* reflection with $h+k+l \neq 2n$ was detected. This fact is illustrated by the ED pattern

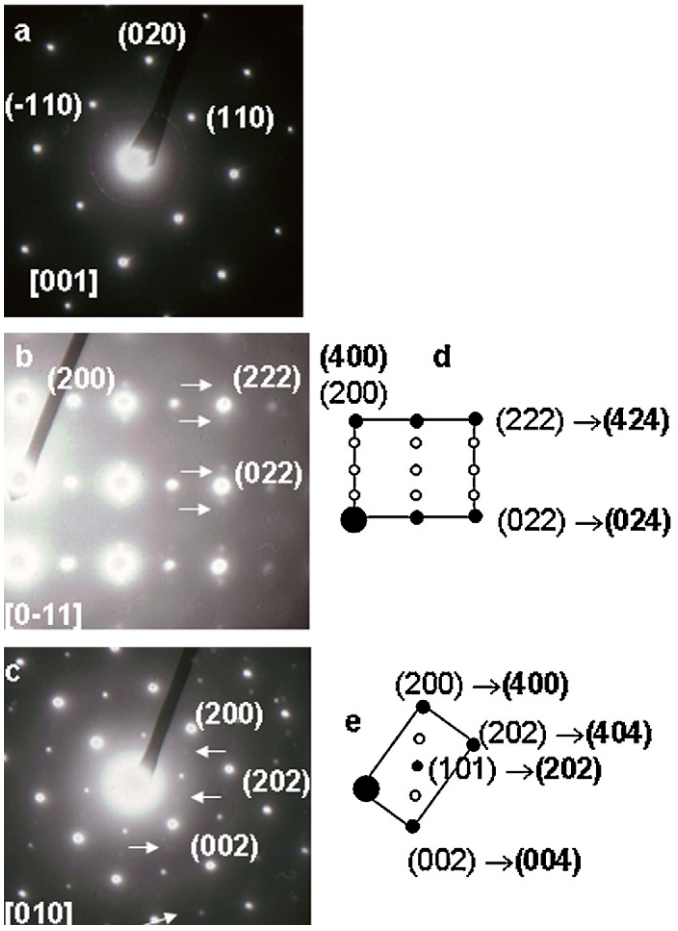

Fig. 1. ED patterns taken at RT along (a) [0 0 1], (b) [0 −1 1] and (c) [0 1 0] zone axes. (d) and (e) Schematic drawings of the ED patterns.

along the zone axis [0 −1 1], gathered in Fig. 1(b), where the (1 1 1) reflection is missing [21]. In this ED pattern the presence of a complex system of extra reflections, characteristic of a double modulation is evidenced. The extra reflections can be ascribed to an orthorhombic supercell with parameters $a = 2\sqrt{2}a_p$, $b = \sqrt{2}a_p$, and $c = 4a_p$, but they are very weak, as illustrated by the [0 −1 1] and [0 1 0] ED patterns given in Fig. 1(b) and (c). For the sake of clarity, schematic drawings of the ED patterns are given in Fig. 1(d) and (e) and the indexation of the reflections corresponding to the supercell are written in bold type. Similar results have been reported for other manganites where CO/OO phenomena are present [2,3].

3.2. Structural and magnetic characterization at high temperature

X-ray diffraction patterns were collected between RT and 700 K under an ambient atmosphere and Fig. 2 shows the evolution of the (1 1 0)–(0 0 2) and (2 2 0)–(0 0 4) reflections with temperature between 298 and 550 K. Patterns above 475 K exhibit sharp and symmetric X-ray peaks whereas below this temperature the reflections are split. The X-ray diffraction data were refined by Rietveld profile analysis using the Fullprof suite of programs [32], and using *Ibmm* subcell ($a_p\sqrt{2}$, $a_p\sqrt{2}$, $2a_p$).

These calculations led to an interesting evolution of cell parameters, which is shown in Fig. 3. In the 300–475 K temperature range, the structure exhibits an O-type distortion ($a > b > c/\sqrt{2}$), frequently associated with a cooperative J-T effect in manganites [5,6]. The observed evolution on warming the sample in this temperature range reveals the characteristic lattice deformation associated

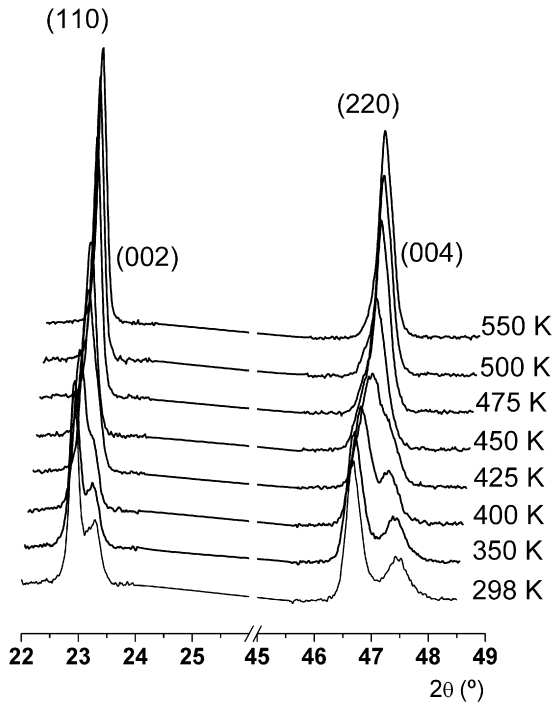

Fig. 2. Selected 2θ intervals of X-ray thermodiffractometric patterns in the 298–550 K temperature range.

to the CO/OO effects: a contraction of the *a* and *b* cell parameters and an expansion of *c* one. Above this temperature, the three parameters increase slowly with the temperature, and the structure becomes pseudocubic.

Moreover, from the analysis of neutron diffraction data at 700 K we find that the sample is tetragonal [7]. The fit is excellent using the tetragonal space group *I4/mcm* ($a^\circ\ a^\circ\ c^-$ in the Glazers terminology) as it is shown in Fig. 4. This symmetry can be simply obtained from the ideal primitive cubic perovskite one by a rotation of [MnO_6] octahedra around the *c* axis by an angle of $\varphi = 5.4^\circ$. The sense of the rotation changes when successive octahedra are considered along the *c* axis. Finally, nuclear peaks of the *I4/mcm* phase split into well separated reflections when the patterns obtained at 700 and 300 K are compared [see, for instance, the (0 0 4)/(2 2 0) reflections in Fig. 5].

The observed structural changes are not simple lattice deformations but actually point to a change of crystal symmetry from tetragonal to orthorhombic. This is illustrated by the splitting

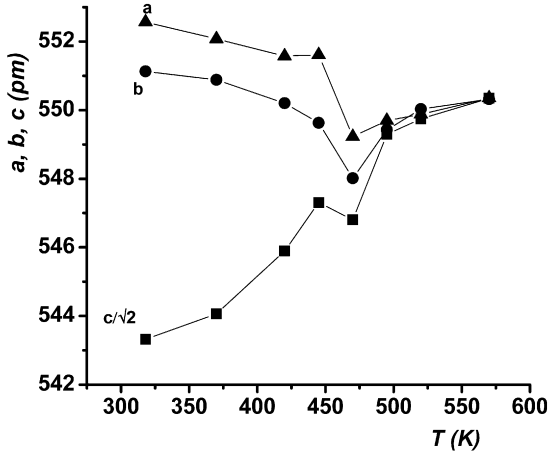

Fig. 3. Variation of cell parameters with temperature from 298 to 550 K.

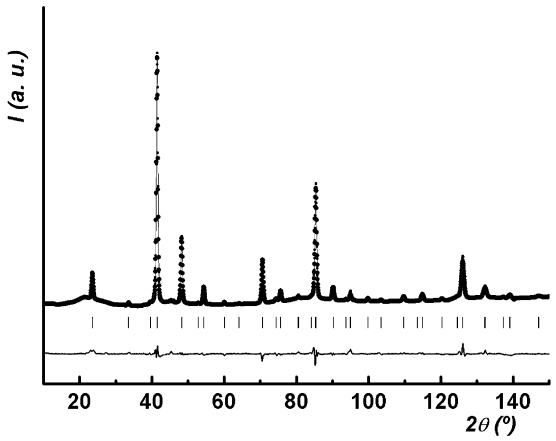

Fig. 4. Rietveld refinement of ND data at 700 K considering the *I4/mcm* SG.

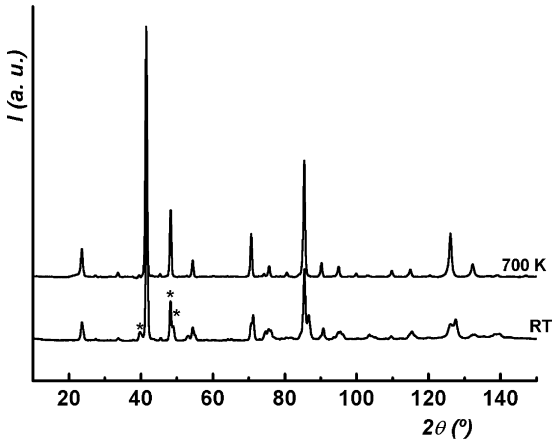

Fig. 5. ND patterns at 300 and 700 K. The reflections (1 0 3), (2 2 0) and (0 0 4) are marked with asterisks.

of the peak which appears at $2\theta \sim 40^\circ$ when the temperature decreases. Thus, the appearance of the (1 0 3) reflection, prohibited in the *I4/mcm* space group, demonstrates the stabilization of the orthorhombic symmetry (Fig. 5). Indeed, considering the orthorhombic *Ibmm* SG we obtained a satisfactory fit for the pattern at 300 K, as is shown in Fig. 6. The structural details obtained by the Rietveld refinements of NDP at different temperatures are gathered in Tables 1 and 2.

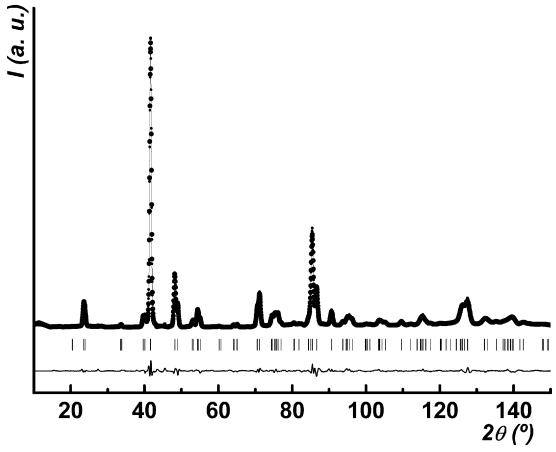

Fig. 6. Rietveld refinement of ND data at 300 K considering the *Ibmm* SG.

Table 1
Structural parameters obtained from Rietveld refinements on ND data at $T = 4$, 80, 300 and 703 K.

T (K)	4	80	300	703
SG	*Ibmm*	*Ibmm*	*Ibmm*	*I4/mcm*
a (Å)	5.514(7)	5.515(8)	5.519(4)	5.513(8)
b (Å)	5.510(2)	5.511(2)	5.516(6)	5.513(8)
c (Å)	7.670(1)	7.671(6)	7.686(6)	7.793(1)
V (Å^3)	233.03(7)	233.13(2)	233.97(8)	236.84(1)
Sr/Bi, x	0.504(7)	0.504(8)	0.505(8)	–
O1, x	0.049(9)	0.049(3)	0.047(1)	–
O2, x	–	–	–	0.262(6)
O2, z	−0.027(1)	−0.027(9)	−0.024(4)	–
μ_{eff} (μ_B)	1.4(1)			
R_B	3.88	3.75	3.00	2.66
R_p	4.29	3.99	3.38	2.61
R_{wp}	5.73	5.29	4.42	3.78

In *Ibmm* SG, the atom positions are: 4a (0 0 0) for Mn/Ti, 4e (x 0 ¼) for Sr/Bi and O1 and 8g (¼ ¼ z) for O2. In *I4/mcm* SG: 4c (0 0 0) for Mn/Ti, 4b (0 ½ ¼) for Sr/Bi, 4a (0 0 ¼) for O1 and 8h (x x +½ 0) for O2.

As revealed by the data included in Table 2, slight differences are found between $d_{Mn/Ti-O1}$ and $d_{Mn/Ti-O2}$ bond distances at RT, which disappear at 700 K. At this latter temperature the octahedral coordination of manganese with oxygen atoms is almost undistorted, leading to six approximately equal distances. However, at RT the two Mn/Ti-O1 distances (along the c axis) become shorter than the four Mn/Ti-O2 distances in the a–b plane by 0.02 Å, suggesting a J-T distortion of the "apically compressed" type. This compression of Mn—O bond distances has been also observed in half-doped manganites [12,15].

On the other hand, it is interesting to note that the bonding mean angle <Mn—O—Mn> for this compound at RT [see Table 2] is very close to that reported for the $Bi_{½}Sr_{½}MnO_3$ phase (Mn—O1—Mn ∼ 164.7° and Mn—O2—Mn ∼ 168.0°) and the high OO/CO transition temperature [17], near 500 K, is slightly higher in the new $BiSrMn_{1.75}Ti_{0.25}O_6$ compound (where Ti^{4+} ions are introduced in the B sublattice). This fact can be explained underlying the very important role of the Bi^{3+} lone pair, as it was pointed by García-Muñoz et al. [17]. These authors suggested that the $6s^2$ lone pair in $Bi_{½}Sr_{½}MnO_3$ could be weakly screened and presumably its electronic density is higher along some Bi-O bonds. This electronic density could be involved in strong covalent interactions via Bi-O bonds, producing an expansion in the Bi^{3+} effective ionic size. In fact, the average interatomic Bi/Sr-O distance [see Table 2] in $SrBiMn_{1.75}Ti_{0.25}O_6$ is larger than in the compound without Ti (2.67 Å). Therefore, we can consider a partial hybridization of the lone pair electrons with some oxygen 2p orbitals, participating in the $e_g(Mn)$—$2p_{\sigma^*}(O)$—$e_g(Mn)$ chemical bonds and leading to an important reduction of the mobility of carriers and giving rise to OO/CO at markedly high temperatures.

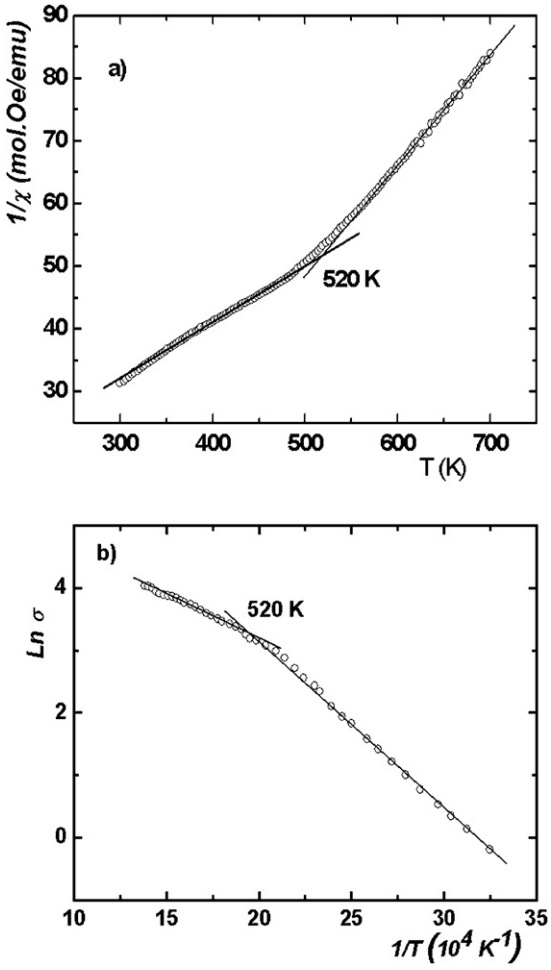

Fig. 7. (a) Temperature dependence of the inverse susceptibility ($1/\chi$). (b) Inverse temperature dependence of the logarithm of the conductivity. The straight lines are the best fits to Arrhenius law for the regions above and below the transition.

3.3. Magnetic and electrical measurements at high temperature

Fig. 7(b) shows the variation of conductivity with $1/T$ above RT for the sample $SrBiMn_{1.75}Ti_{0.25}O_6$, whose main feature is a change of slope at $T > 500$ K. The activation energy value between RT and 520 K is 0.24 eV and decreases down to 0.12 eV for higher temperatures; i.e., there is an evolution towards electronic delocalization as T increases. This behaviour can be related to the above mentioned structural transition in which the octahedral tilting progressively diminishes. On the other hand, at this transition temperature a change of slope in the reciprocal susceptibility is observed, as

Table 2
Bond distances (Å) and angles (°) from Rietveld refinements on ND data at different temperatures.

T (K)	4	80	300	703
SG	*Ibmm*	*Ibmm*	*Ibmm*	*I4/mcm*
$d_{Sr/Bi—O1}$	2.507(4)	2.507(6)	2.526(5)	2.756(4) × 4
	2.770(4) × 2	2.771(1) × 2	2.773(6) × 2	
	3.006(3)	3.008(2)	2.993(9)	
$d_{Sr/Bi—O2}$	2.894(6) × 4	2.893(3) × 4	2.886(6) × 4	2.821(5) × 4
	2.581(4) × 4	2.582(4) × 4	2.596(1) × 4	2.693(7) × 4
$<d_{Sr/Bi—O}>$	2.746(2)	2.747(6)	2.749(3)	2.756(5)
$d_{M—O1}$ [a] × 2	1.936(4)	1.937(8)	1.939(1)	1.948(3)
$d_{M—O2}$ × 4	1.960(8)	1.960(1)	1.960(1)	1.951(2)
$<d_{M—O}>$	1.952(1)	1.952(3)	1.953(1)	1.950(2)
$\theta_{M—O1—M}$	163.9(5)	163.8(4)	164.5(1)	180.0
$\theta_{M—O2—M}$	167.8(4)	167.8(1)	169.02(1)	174.6(1)

[a] M = Mn/Ti.

Table 3
Theoretical magnetic moments (μ_B) from the different analyzed models.

	$\mu_{theor.}$	S_1	S_2
Ionic model	5.93	Mn^{3+} – 2	Mn^{4+} – 3/2
ZPO model	7.30	Mn^{3+} – 2	$Mn^{3.5+}$ – 7/2
$1Mn^{4+} + 2Mn^{3+}$, clusters	8.67	Mn^{4+} – 3/2	Mn_3 – 11/2
$1Mn^{4+} + 3Mn^{3+}$, clusters	9.51	Mn^{4+} – 3/2	Mn_4 – 15/2

shown in Fig. 7(a). Therefore, it is interesting to note that a strong interdependence between magnetic and electrical properties with the structural transition is clearly evidenced for $SrBiMn_{1.75}Ti_{0.25}O_6$.

By fitting the magnetic data to a Curie law below and above the transition temperature, the effective paramagnetic moments of $\mu_{eff} = 9.34\ \mu_B$ ($T < 500$ K) and $\mu_{eff} = 6.82\ \mu_B$ ($T > 500$ K) are obtained. An increase of μ_{eff} in the low temperature range is a characteristic feature of half-doped manganites exhibiting CO, and a proper interpretation was given within the framework of the Zener polaron model [25]. In such phases the value of μ_{eff} found above the transition is consistent with a mixture of Mn^{3+} and Mn^{4+} cations (i.e., with an ionic model); and the value found below the transition matches the value that one can expect for coexistence of Zener polarons and Mn^{3+} ions [17,25]. However, in our case, as can be seen in Table 3, the observed μ_{eff} above and below the transition temperature are much larger than the expected theoretical values. This enhanced μ_{eff} can be explained by the presence of magnetic clusters in the paramagnetic state, as theoretically predicted [33] and experimentally observed for several manganites [5,14]. Like in other manganite systems, it could be considered here that the Mn^{4+} ions constitute the core of the clusters (i.e., one hole shared by several Mn^{3+} ions) and thus the expected μ_{eff} of the sample is calculated by the following equation [5]:

$$\mu_{eff}^{theo} = \sqrt[g]{x_{S_1} S_1(S_1+1) + x_{S_2} \cdot S_2(S_2+1)}$$

in which S_1 and S_2 refer to the spin values given in Table 3, g is the Landé factor, equal to 2, and x_{S_1} and x_{S_2} indicate the amount of cations and clusters with each spin, respectively. Among the different possibilities gathered in Table 3, the comparison of the experimental and theoretical μ_{eff} values at $T < 500$ K, suggests that the $1Mn^{4+} + 3Mn^{3+}$ combination agrees the best with the observed values. This fact implies that only a fraction of the manganese cations are involved in the clustering, similarly to that reported for $La_{7/8}Sr_{1/8}MnO_3$, in which Mn^{3+} concentration is greater than the Mn^{4+} one, as also occurs in our case [5,6].

Moreover, at $T > 500$ K, where the $SrBiMn_{1.75}Ti_{0.25}O_6$ phase shows a tetragonal symmetry, the μ_{eff} value still remains slightly higher than the corresponding to isolated Mn^{3+} and Mn^{4+} ions, indicating the existence of superparamagnetic clusters, which are progressively shrunk.

Therefore, from the above results we can conclude that each hole-type charge carrier associated with a Mn^{4+} ion is embedded into a locally ferromagnetic environment, extending to the nearest-neighbour sites. Thus, the charge transfer depends on the orbital configuration between Mn^{4+} and its nearest neighbours.

3.4. Magnetic and electric measurements at low temperature

The variation of conductivity with temperature below RT for the $SrBiMn_{1.75}Ti_{0.25}O_6$ sample is shown in Fig. 8. Conductivity values are relatively low and no jumps are observed in the explored low temperature range, in concordance with the high T_{CO} found in this compound; i.e., at RT the compound still presents charge ordering.

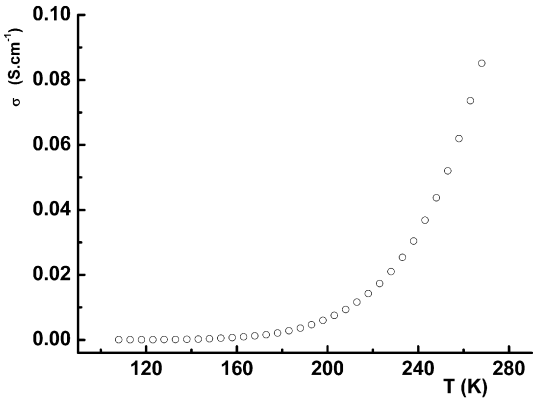

Fig. 8. Temperature dependence of the conductivity, σ.

The thermal dependence of the magnetic susceptibility at 500 Oe, between 4 and 300 K, is displayed in Fig. 9. The magnetic susceptibility shows a cusp-like anomaly at around 40 K that suggests the existence of a frustrated state at low temperatures. This assumption is also supported by the hysteretic behaviour of the magnetization at 5 K (see Fig. 9(b)). The appearance of that frustration can be understood by considering the introduction of Ti^{4+} at the B-sites, thus breaking the coherence of the long-range magnetic interactions. These results agree well with a weak antiferromagnetic (AFM) component of 1.4 μ_B at 4 K, as discussed below.

3.5. Structural and magnetic characterization at low temperature

The structural study displayed above [sections A and B] was based on the diffraction data taken between RT and 700 K. In this section we present a complementary neutron diffraction study at the low temperature region. Neutron diffraction patterns were collected at 80 and 4 K using the D2B diffractometer in high resolution mode. The low angle-region of the NPD patterns at RT, 80 and 4 K are shown in Fig. 10.

The patterns obtained at 80 and 4 K reveal the presence of magnetic reflections [(0 0 1) and (1 1 1)], typically associated with the A-type magnetic structure. Therefore, we have refined the ND patterns by assuming an A-type magnetic ordering for the $BiSrMn_{1.75}Ti_{0.25}O_6$ phase. The refined NPD pattern at 4 K is shown in Fig. 11. The obtained results from both refinements, at 4 and 80 K, are given in Tables 1 and 2. The ordered magnetic moment found for this phase [1.4(1) μ_B per Mn ion] is clearly smaller that

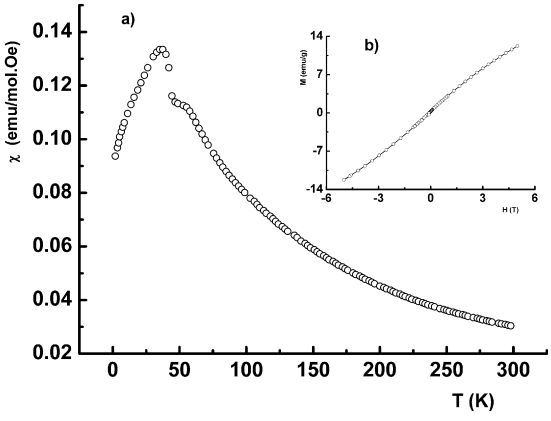

Fig. 9. (a) Magnetic susceptibility vs. temperature at 500 Oe. (b) Magnetization vs. magnetic field at 4 K.

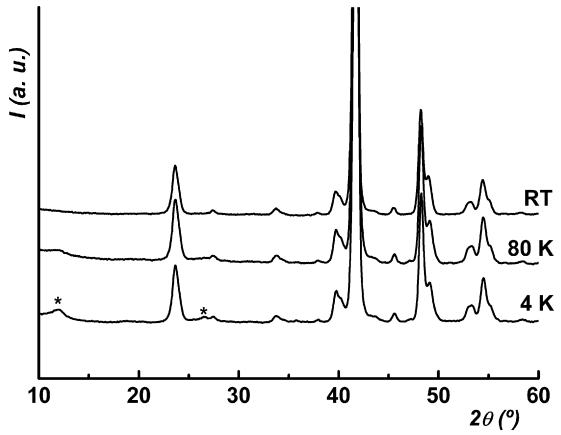

Fig. 10. ND patterns at 4, 80 and 300 K. The magnetic reflections (0 0 1) and (1 1 1) are marked with asterisks.

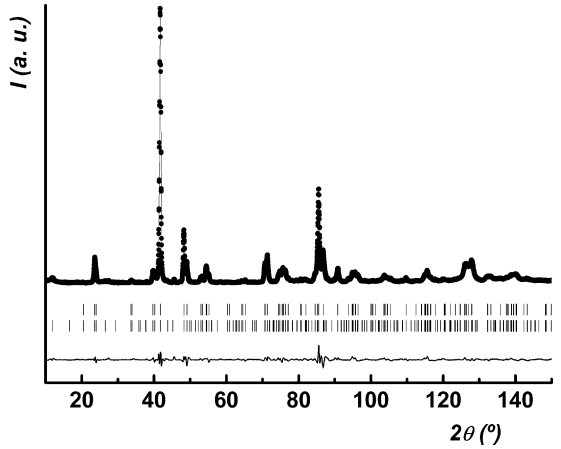

Fig. 11. Rietveld refinement of ND data and magnetic phase at 4 K considering the *Ibmm* SG.

the value expected for a complete ordering, and points to frustration phenomena of the magnetic interactions as a consequence of the presence of Ti^{4+} cations, which are partially occupying the Mn positions.

4. Conclusions

A detailed study of the new manganite derivative, $BiSrMn_{1.75}Ti_{0.25}O_6$, has been carried out showing interesting structural, electric and magnetic features of this phase. From the structural point of view, diffraction data evidence a tetragonal structure *I4/mcm* above T_{CO} and at lower temperatures, a transition to an orthorhombic symmetry, *Ibmm*, takes place. Such a transition is detected by splits in the X-ray and neutron diffraction peaks. Moreover, the magnetic susceptibility obtained between RT and 700 K indicates that the effective moments enhance from their expected theoretical values both in tetragonal and orthorhombic phases, suggesting the presence of magnetic clusters as well as that they depend on the J-T distortions.

It is noteworthy that the phase segregation phenomena reported to exist in some Sr doped manganites [18] have not been evidenced in our sample.

The low-temperature structural and transport properties of the title phase show an A-type magnetic ordering associated with the OO. This assumption agrees well with the observed compression of the *c* parameter, as temperature is decreased, leading to an apical distortion of the Mn/TiO_6 octahedra.

In general terms, the above results also support the differences, previously reported in the literature, between the rare earth manganites with $x \sim 0.5$ and the Bi-containing systems. The rare earth derivatives typically show an A-type magnetic structure and are described as "metallic antiferromagnets" in which the FM planes are conducting. In contrast, this picture is not valid in Bi-substituted manganites, as they display much higher resistivity values evidencing an important electronic localization. As it was suggested by some authors [18,19], these points can be understood taking into account that the $6s^2$ lone-pair of Bi^{3+} induces a dominant effect in these phases, causing a great reduction in the manganese e_g electrons mobility. Local distortions or even hybridization between 6s-Bi-orbitals and 2p-O-orbitals can take place [19] due to a preferential orientation of the $6s^2$ lone-pair towards the surrounding oxide anions.

In conclusion, X-ray and neutron diffraction data, as well as conductivity and magnetization measurements, reveal evidences of a remarkably high orbital and charge ordering temperature in $BiSrMn_{1.75}Ti_{0.25}O_6$. These results seem to support the interpretation previously proposed [17] concerning the important role of the Bi $6s^2$ lone-pair in the CO/OO ordering. This feature is revealed in $BiSrMn_{1.75}Ti_{0.25}O_6$ to be crucial as the introduction of Ti^{4+} in manganese sites does not seem to affect the transition temperature.

Acknowledgements

We acknowledge financial support from Spanish Ministerio de Ciencia e Innovación – Grant MAT2010-20117. Authors are grateful to the ILL and CAI centers of UCM (neutron diffraction facilities and XRD and electron microscopy, respectively).

References

[1] J.M. De Teresa, M.R. Ibarra, P.A. Algarabel, C. Ritter, C. Marquina, J. Blasco, J. García, A. del Moral, Z. Arnold, Lett. Nat. (1997) 386.
[2] Y. Tomioka, X.Z. Yu, T. Ito, Y. Matsui, Y. Tokura, Phys. Rev. B 80 (2009) 094406.
[3] P.R. Sagdeo, N.P. Lalla, A.V. Narlikar, D. Prabhakaran, A.T. Boothroyd, Phys. Rev. B 78 (2008) 174106.
[4] P.R. Sagdeo, S. Anwar, N.P. Lalla, Solid State Commun. 137 (2006) 158.
[5] J. Nogués, V. Skumryev, J.S. Muñoz, B. Martinez, J. Fontcuberta, L. Pinsard, A. Revcolevschi, Phys. Rev. B 64 (2001) 024434.
[6] P. Wagner, I. Gordon, S. Mangin, V.V. Moshchalkov, Y. Bruynseraede, L. Pinsard, A. Revcolevschi, Phys. Rev. B 61 (2000) 529.
[7] C. Frontera, J.L. García-Muñoz, A. Llobet, C. Ritter, Phys. Rev. B 62 (2000) 6822.
[8] A. Llobet, J.L. García-Muñoz, C. Frontera, C. Ritter, Phys. Rev. B 60 (1999) R9889.
[9] J.B. Goodenough, Phys. Rev. 100 (1955) 564.
[10] E.D. Wolan, W.C. Koehler, Phys. Rev. 100 (1955) 545.
[11] G.C. Milward, M.J. Calderon, P.B. Littlewood, Nature (London) 433 (2005) 607.
[12] B. Raveau, M. Hervieu, A. Maignan, Phys. Rev. B 62 (2000) 6820.
[13] H. Kawano, R. Kajimoto, H. Yoshizawa, Y. Tomioka, H. Kuwahara, Y. tokura, Phys. Rev. Lett. 78 (1997) 4253.
[14] R.P. Borges, F. Ott, R.M. Thomas, V. Skumryev, J.M.D. Coey, J.I. Arnaudas, L. Ranno, Phys. Rev. B 60 (1999) 12847.
[15] P.G. Radaelli, D.E. Cox, M. Marezio, S.-W. Cheong, Phys. Rev. B 55 (1997) 3015.
[16] N. Biškup, A. de Andrés, J.L. Martínez, C. Perca, Phys. Rev. B 72 (2005) 024115.
[17] J.L. García-Muñoz, C. Frontera, M.A.G. Aranda, A. Llobet, C. Ritter, Phys. Rev. B 63 (2001) 064415.
[18] C. Frontera, J.L. García-Muñoz, M.A.G. Aranda, C. Ritter, A. Llobet, M. Respaud, J. Vanacken, Phys. Rev. B 64 (2001) 054401.
[19] J.L. García-Muñoz, C. Frontera, M.A.G. Aranda, C. Ritter, A. Llobet, M. Respaud, M. Gorian, H. Rakoto, O. Masson, J. Vanacken, J.M. Broto, J. Solid State Chem. 171 (2003) 84.
[20] M. Hervieu, A. Maignan, C. Martin, N. Nguyen, B. Raveau, Chem. Mater. 13 (2001) 1356.
[21] M. Hervieu, S. Malo, O. Perez, P. Beràn, C. Martin, G. Baldinozzi, B. Raveau, Chem. Mater. 15 (2003) 523.
[22] M. Giot, P. Beràn, O. Perez, S. Malo, M. Hervieu, B. Raveau, M. Nevriva, K. Knizek, P. Roussel, Chem. Mater. 18 (2003) 3225.
[23] F. Damay, C. Martin, M. Hervieu, A. Maignan, B. Raveau, G. André, F. Bourée, J. Magn. Magn. Mater. 184 (1998) 71.
[24] J.L. García-Muñoz, C. Frontera, M. Respaud, M. Giot, C. Ritter, X.G. Capdevila, Phys. Rev. B 72 (2005) 054432.

[25] C. Frontera, J.L. García-Muñoz, M.A.G. Aranda, M. Hervieu, C. Ritter, Ll. Mañosa, X.G. Capdevila, A. Calleja, Phys. Rev. B 68 (2003) 134408.
[26] C.N.R. Rao, A. Arulraj, P.N. Scintosh, A.K. Cheethan, Chem. Mater. 10 (1998) 2714.
[27] P.M. Woodward, D.E. Cox, T. Vogt, C.N.R. Rao, A.K. Cheethan, Chem. Mater. 11 (1999) 3528.
[28] B. Liu, Z. Jiang, B. Ding, F. Chen, C. Xia, J. Power Sources 196 (2011) 999–1005.
[29] O. Toulemonde, I. Kovsen, F. Mesguich, E. Gaudin, Solid State Sci. 10 (2008) 476.
[30] C.M. Xiong, J.R. Son, R.W. Li, S.Y. Zhang, T.Y. Zhao, B.G. Shen, J. App. Phys. 95 (2004) 1336.
[31] H.M. Rietveld, J. Appl. Cryst. 2 (1969) 65.
[32] J. Rodriguez-Carvajal, Phys. B.: Condens. Matter 192 (1993) 55, http://www.ill.eu/sites/fullprof/index.html.
[33] M.D. Coey, M. Viret, L. Ranno, K. Ounadjala, Phys. Rev. Lett 75 (1995) 3910.